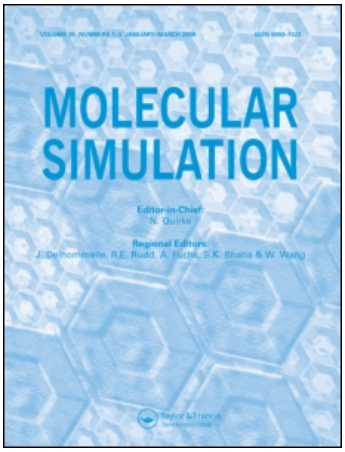

Molecular Simulation
Publication details, including instructions for authors and subscription information:
http://www.informaworld.com/smpp/title~content=t713644482

Simulation of Deposition of Wax to Iron Oxide Surfaces

Miguel A. San-miguel[a]; P. Mark Rodger[a]
[a] Department of Chemistry, University of Warwick, Coventry, UK

To cite this Article San-miguel, Miguel A. and Rodger, P. Mark(2001) 'Simulation of Deposition of Wax to Iron Oxide Surfaces', Molecular Simulation, 26: 3, 193 — 216
To link to this Article: DOI: 10.1080/08927020108028293
URL: http://dx.doi.org/10.1080/08927020108028293

Molecular Simulation, 2001, Vol. 26, pp. 193–216
Reprints available directly from the publisher
Photocopying permitted by license only

SIMULATION OF DEPOSITION OF WAX TO IRON OXIDE SURFACES

MIGUEL A. SAN-MIGUEL* and P. MARK RODGER†

Department of Chemistry, University of Warwick, Coventry CV4 7AL, UK

(Received March 2000; accepted March 2000)

Molecular dynamics techniques have been used to model the processes associated with the deposition of alkanes on a hematite surface, and the subsequent growth of an alkane crystal. First we have obtained a relaxed (0001)-hematite surface; this is believed to be the most common surface exhibited on the pipeline walls. Subsequently, the adsorption of two different linear alkanes has been examined: C_{12} and C_{28}. The principal adsorption site for both has been determined and consisted of the molecule lying between two parallel rows of iron atoms. The subsequent addition of alkane molecules generates a crystalline structure, which corresponds closely with C_{28} crystal growth along the (010) direction.

Keywords: Molecular dynamics; Iron oxide surface; Wax; Deposition

1. INTRODUCTION

There are various phenomena that affect the efficiency of transport processes in oil and gas pipelines including corrosion, scale and wax deposition, and clathrate hydrate formation. Protecting pipelines from all these problems constitutes an important problem for the industry. There have been many experimental studies focusing on each of these aspects separately, however theoretical treatments are more rare. Moreover, there have been very few attempts to understand the interplay between these problems and the methods used to solve them. This interdependence does exist, and may be either synergistic or competitive. A good example of the latter is the relation between corrosion inhibition and wax deposition, where it has been

*Corresponding author. e-mail: M.A.San-Miguel-Barrera@warwick.ac.uk
†e-mail: P.M.Rodger@warwick.ac.uk

observed that the use of chemical compounds that inhibit corrosion can promote wax deposition [1]. While this does enhance their ability to prevent corrosion, it may still reduce pipeline efficiency. As a first step towards understanding this dependence, we present here an analysis of the separate problem of the wax deposition on Fe_2O_3 hematite surface. This will provide a base line from which corrosion inhibitor effects can be determined.

Molecular dynamics (MD) and Monte Carlo (MC) constitute reliable techniques to model this sort of problem. In fact, they have been used to study hydrocarbon adsorption on an aluminium oxide surface [2, 3], on metal surfaces such as Pt [4–6], Au [7–9] and W [10], and on graphite [11–14]. In this paper we present results of a MD study of adsorption and subsequent growth of *n*-alkanes deposits on a relaxed Fe_2O_3 hematite surface. Two different hydrocarbons (C_{12} and C_{28}) have been studied in order to determine the possible mechanism by which the formation of a monolayer and the subsequent crystal growth takes place.

2. THE SYSTEM AND SIMULATION DETAILS

2.1. Surface

Pipelines are made of mild steel. It is known that under common work conditions an oxide film on the iron surface is formed, which mostly presents a hematite structure [15]. The structure of the hematite is corundum-type (space group $R\bar{3}c$, with two and six formula units in the primitive rombohedral and in the hexagonal unit cells, respectively). The parameters for the hexagonal cell are $a = b = 5.0347\,\text{Å}$, $c = 13.7473\,\text{Å}$, $\alpha = \beta = 90°$, $\gamma = 120°$, as determined by X-ray diffraction at ambient temperature and high pressure [16]. This structure consists of hexagonal close packed (hcp) anions, with two thirds of the resulting octahedral sites being occupied by cations. Up till now, only a few theoretical studies on this system have been reported and they have focussed on electronic properties [17–20].

Experiments have shown that the (0001) surface is one of the most stable surfaces, and reconstruction is observed only at high temperatures [21–24]. It is reasonable to start with the assumption that the iron surface in the pipelines is oxidised and the adsorption processes take place on this non-reconstructed termination. The validity of this assumption is currently being tested in work in progress.

Cations or anions can terminate this surface. In this paper we consider a cationic termination; this has been supposed to be the most abundant and

so the only one considered to date. According to this model, every surface three-fold coordinated cation could have three H_2O molecules adsorbed; depending on the pH of the system these water molecules could be replaced by OH^- groups. However, at this stage of our study we will only consider the surface without H_2O and OH^-.

For this termination there is predicted to be a strong contraction of the surface layers after cleaving the crystal [25–28]. A similar phenomenon has been observed experimentally in Al_2O_3 and Cr_2O_3. Figure 1 shows this relaxation schematically. It is important to obtain an adequate model of this surface after the relaxation, because the structure is quite different from the ideal surface and the results would otherwise be unrealistic. Unfortunately there are no experimental data about how the layers are compressed with which to compare, although some theoretical estimates have been made [27, 28].

In order to get a representative model of this surface, we performed molecular dynamics simulations of a slab which consisted of 1920 particles packed in a hexagonal box of $a = b = 40.2776$ Å and $c = 13.7473$ Å, according to the experimental dimensions of the crystal [16]. Periodic boundary conditions along three directions were employed, although a vacuum gap of 60 Å was included along the c direction to create the surfaces and permit relaxation of the slab. Both surfaces of the slab were cation terminated and equivalent.

Classical molecular dynamics simulations were undertaken using DL_POLY [29]. Calculations were performed in the NVT ensemble, using a Nose-Hoover thermostat with a thermal parameter of 0.1 and a time step of 1 fs. In order to get the relaxed structure simulations were carried out at very low temperature (*e.g.*, 2 K) instead of using an energy minimisation procedure. It has been found that this technique leads to structures

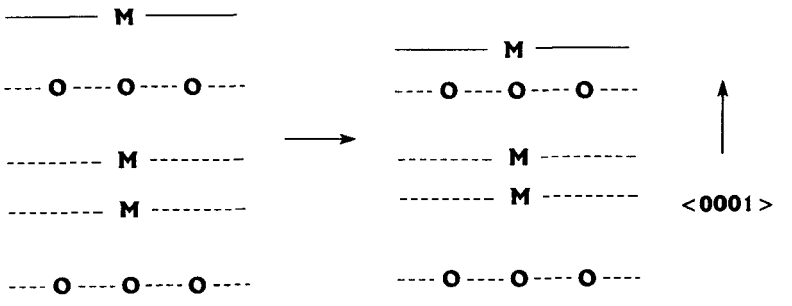

FIGURE 1 Relaxed structure for the (0001)-hematite surface.

that correspond well to those obtained by means of other minimisation methods and is more efficient than minimisation within DL_POLY. The simulation consisted of a 10 ps trajectory during which the velocity of the particles were rescaled every 3 steps, followed by a further 10 ps trajectory to verify the system had reached equilibrium and for statistical analysis.

The interaction potential function for the Fe_2O_3 is given by:

$$V(r_{ij}) = \frac{q_i q_j e^2}{r_{ij}} + \frac{e^2}{n(\sigma_i + \sigma_j)} \left(\frac{\sigma_i + \sigma_j}{r_{ij}} \right)^9$$

where q_i are the effective charges obtained from periodic *ab initio* calculations [20], and σ_i the ionic radii [30]. The second term is called a Pauling-type potential and describes the short-range interactions. The first term corresponds to the long-range interactions and was implemented using the Ewald method. A cut-off radius of 13 Å was used in both short-range and long-range interactions. A charge of 2.6175 e was used for iron and -1.745 e for oxygen atoms, according to the values obtained from *ab initio* periodic unrestricted Hartree-Fock calculations by Catti *et al.* [20] Ionic radii were 0.785 Å for Fe and 1.24 Å for O. The Ewald parameter α was set to 0.44 and the reciprocal space vector used were $k_x = k_y = 8$ and $k_z = 13$, which were adequate to reach convergence in the Ewald sum within a reasonable computer time.

The surface energies can be calculated as:

$$\gamma_{\text{surf}} = \frac{E_{\text{slab}} - E_{\text{bulk}}}{2A}$$

where E_{slab} is the potential energy of the slab system, E_{bulk} is the potential energy of an equivalent number of Fe_2O_3 molecules in the bulk, and A is the surface area. The factor 2 arises because there are two equivalent surfaces in the calculation.

Relaxed surface energies, γ_{rlx}, were calculated from the energies of the bulk and the slab after relaxation ($E_{\text{rlx-bulk}}$ and $E_{\text{rlx-slab}}$), and unrelaxed

TABLE I Surface energies for (0001) surface of hematite

	$\gamma_{surf}/J\ m^{-2}$		
	This work	MM^{27}	MD^{28}
Unrelaxed	4.7	5.3	4.2
Relaxed	1.9	1.5	1.6

values, $\gamma_{\text{non-rlx}}$, from $E_{\text{rlx-bulk}}$ and the energy of the slab without relaxation. Table I shows the values of surface energy, together with comparable values from the literature obtained using minimisation techniques (MM) [25, 27] or molecular dynamics simulations (MD) [28]. Our values are comparable with the other calculations and the magnitude of the decrease in energy on relaxation indicates the system is highly stabilised by this process.

Table II quantifies the contraction of the uppermost layers. It can be seen that the first Fe—O distance is reduced by around 50% with respect to the bulk. Our simulations do not predict any change for the second Fe—O distance. The Fe—Fe distance decreases by 40%, while the third Fe—O distance is 10% bigger than in the bulk. The last is the biggest percentage difference between our results and those of Wasserman *et al.* [28] although in absolute terms the difference is small (0.1 Å)

Since this relaxed surface is very stable and suffers neither surface reconstruction at moderate temperature nor other alterations during the adsorption of representative molecules [31], the iron and oxygen positions were fixed to the relaxed surface structure in all the surface adsorption simulations reported here; this resulted in substantial savings in computational time.

2.2. Wax

Waxes are microcrystalline aggregates of alkane molecules. For many oil systems waxes form from the C_{20}—C_{36} fraction. In this work we have focused on C_{28} as a representative case.

C_{28} has been found to be monoclinic and the lattice parameters are $a = 5.57$ Å, $b = 7.42$ Å, $c = 38.19$ Å, $\alpha = 90°$, $\beta = 119.1°$, $\gamma = 90°$ [32]. The unit cell contains two molecules. Figure 2 shows the structure and the

TABLE II Interplanar distances after relaxation of the slab at 2K. Figures in parenthesis indicate the change as a percentage of the bulk values. For the subsequent layers, (*i.e.*, those not indicated in this table), the distances are the same as for the bulk structure

		d/Å	
Interlayer		*This work*	*Ref.* 28
Surface	Fe—O	0.4 (−55)	(−49)
	O—Fe	0.9 (0)	(−3)
	Fe—Fe	0.3 (−40)	(−41)
	Fe—O	1.0 (+10)	(+21)
Bulk	Fe—Fe	0.5	–
	Fe—O	0.9	–

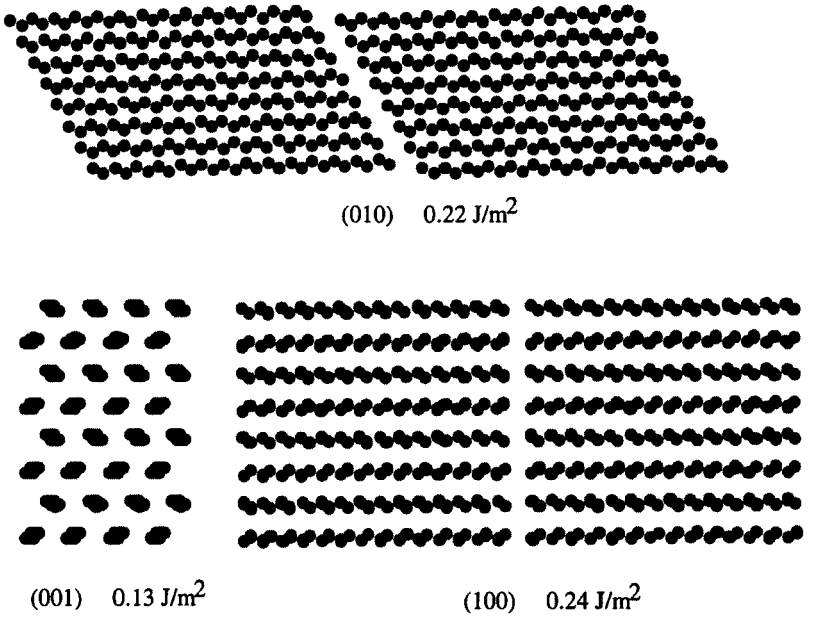

FIGURE 2 Main surfaces and corresponding surface energies for the C_{28} crystal.

corresponding surface energies of the main surfaces for crystalline C_{28}. Surface energies were calculated by carrying out MD simulations at $T = 2\,K$ for the bulk crystal and each of the three surfaces. Surface calculations were performed with slabs of several different thicknesses to ensure convergence of the surface energies [33]. The (001) surface has a substantially lower energy than do the others, which indicates that it is the most stable surface in the series and so is likely to dominate the equilibrium morphology of C_{28} crystals. The (010) and (100) surfaces have similar energies, both of which are higher than the (001) surface; it is expected that these will be the faces along which crystal growth will occur, as they give the lowest attachment energies [33].

Since the length of the alkane molecules extends almost along the whole Fe_2O_3 surface, the periodic boundary conditions in this C_{28} system do involve each molecule interacting with itself, and this could generate artefacts in the results. Simulations with two sets of C_{28} molecules were found too expensive in cpu time for an exhaustive study. We have therefore sought to evaluate the effect of this imposed periodicity using two sets of shorter alkanes. Due to the structural differences between odd and even chains, and taking into account that C_{14} is incommensurate with the Fe_2O_3

surface, we have chosen to use C_{12} for this purpose. The crystal structure of C_{12} is triclinic and the spatial group is P1 [34], and so isolated crystals exhibit a morphology quite different from C_{28}. However, the presence of the hematite surface will impose a spatial order akin to that found in C_{28} molecules, and so the C_{12} adsorption is likely to be analogous to that for the longer alkane, especially for the first few add-layers.

The interactions in the wax were described by a united-atom model. In this model the methyl and methylene groups are represented by a single interaction site located at the position of each carbon atom. The parameters were derived from reference 35, but with the bending and torsion angle parameters modified to get a better description of bulk structures for C_{20} to C_{36} crystals [32]. All potential parameters are listed in Table III.

TABLE III Parameters used in the united-atom (UA) model for alkane chains

Intramolecular Potential Functions	
Bond Potential:	Constrained
Valence Angle Potential:	$U(\theta_{jik}) = (k/2)\ (\theta_{jik} - \theta_0)^2$
Dihedral Angle Potential:	$U(\theta_{jikn}) = A_i[1 + \cos(m_i\theta_{jikn})] \quad i = 1,6$
Intermolecular Potential Functions	
Short Ranged Potential:	$U(r_{ij}) = 4\varepsilon[(\sigma/r_{ij})^{12} - (\sigma/r_{ij})^6]$
Long Ranged Electrostatic Potential:	$U(r_{ij}) = (q_i q_j e^2/r_{ij}) + (e^2/n(\sigma_i+\sigma_j))\ (\sigma_i+\sigma_j/r_{ij})^9$

TABLE IIIA Bond parameters

Bond	*Length* (Å)
C—C	1.53

TABLE IIIB Valence angle parameters

Bond	k ($kJ\,mol^{-1}\,rad^{-2}$)	θ (*deg*)
C—C—C	520.0	112.5

TABLE IIIC Dihedral angle parameters

C—C—C—C torsion, i	m_I	A_I
1	0	−9.840
2	1	9.823
3	2	6.560
4	3	10.607
5	4	3.280
6	5	1.968

TABLE IIID Short ranged parameters

Pair	$\varepsilon(kJ\ mol^{-1})$	σ (Å)
CH_3—CH_3	0.64230	3.7400
CH_3—CH_2	0.62009	3.8230
CH_2—CH_2	0.59864	3.9230
Fe—CH_3	0.38450	3.8920
O—CH_2	0.37120	3.9835
O—CH_3	0.50710	3.3870
O—CH_2	0.48960	3.4785

TABLE IIIE Long ranged parameters

Atom	$q(e)$	σ (Å)
Fe	2.6175	0.785
O	−1.7450	1.240
CH_2	0.0	–
CH_3	0.0	–

3. RESULTS AND DISCUSSION

3.1. Adsorption Site

A range of possible surface adsorption sites has been examined for both alkanes. A C_{28} molecule was initially located on the surface and lying between two rows of protruding Fe atoms. Very low temperature MD was then used to relax the structure. A range of alternative starting configurations, where the alkane long axis made an angle with the rows of surface Fe atoms in the range 0–60° was also considered. Given the hexagonal symmetry of this surface, this defines the full range of unique angles. A structure with minimum total energy was found when the molecule lay in between two parallel iron rows (see Fig. 3). It can be seen that the adsorption geometry involves a zigzag between the protruding iron atoms and in a plane parallel to the surface. The adsorption energy, defined as $E_{ads} = E_{surf+wax} - E_{surf} - E_{wax,}$ was $-173.9\,kJ\,mol^{-1}$; the same geometry was found for C_{12} and the E_{ads} was $-76.9\,kJ\,mol^{-1}$. Both of these E_{ads} are equivalent to $-6.3\,kJ\,mol^{-1}$ per carbon site.

3.2. Crystal Growth

Monomer adsorption is likely to be an important stage in preparing for wax formation on a pipe surface, however it is the formation of crystalline layers that really marks the beginning of wax deposition. We have considered two different approaches in order to study the forma-

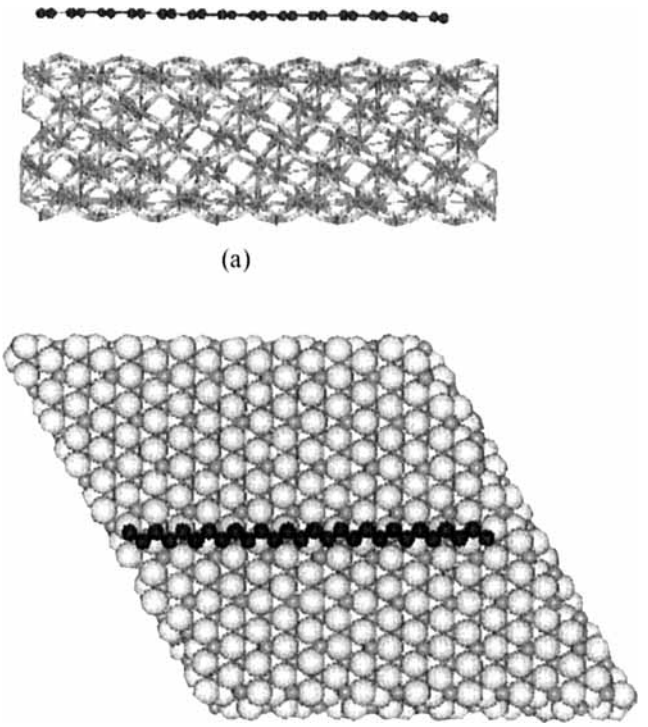

FIGURE 3 C_{28} molecule adsorbed on (0001)-hematite surface. Side (a) and top (b) views of the most favourable adsorption geometry. Carbon atoms are in black, iron atoms in orange and oxygen atoms in grey. (See Color Plate I).

tion of alkane monolayers on hematite surface. The first one comes from the intuitive idea of allocating an alkane molecule between two iron rows and we have called this 'ideal deposition'. The second procedure corresponds to a more realistic process in which every molecule is initially deposited on the surface in a random position, and it is the collective interactions with the environment that induce ordering and the crystal formation. We will refer to this mechanism as 'random deposition'.

3.2.1. Ideal Deposition

As we mentioned above, the initial configuration for simulations of an alkane layer adsorbed on hematite was obtained by placing an alkane

molecule between every two iron rows, with the zig-zag plane of the alkane oriented parallel to the surface. For the hematite surface used here, eight C_{28} molecules were added to give the maximal coverage. Two starting structures were considered for C_{12}: the first had a single block of eight C_{12} molecules; the second involved two blocks of eight molecules separated by a gap of 6 Å.

The adsorbed layers were relaxed by performing MD at very low temperature (2 K) for 30 ps while keeping the hematite slab immobile. After simulating for a few ps the molecules were observed to rotate about their long axis so that the zig-zag plane was no longer parallel to the surface (this effect will be described below). A further three layers were added in successive stages, allowing relaxation of all the system (except Fe_2O_3 surface) at 2 K for 30 ps after adding each new layer. The final results are shown in Figure 4. At every stage an additional 50 ps simulation was performed at 300 K to study the behaviour of the system at room temperature.

The simulations were used to calculate the density of carbon atoms along the surface normal, and the results are depicted in Figure 5. The figures

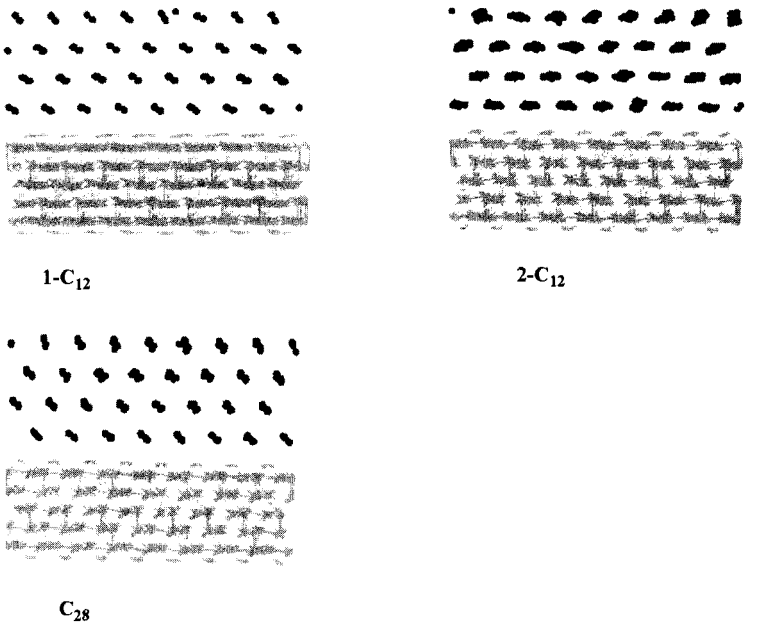

FIGURE 4 Side views of a single block (1-C_{12}) and two blocks (2-C_{12}) of thirty two C_{12} molecules and a single block of thirty two C_{28} molecules after relaxation at 2 K. Carbon atoms are in black and oxide surface in orange (Fe) and grey (O). (See Color Plate II).

show bands at the positions of the layers, with most of the bands consisting of a doublet. The interlayer distance can be estimated from the separation between the two middle points of consecutive doublets. This distance was found to be 3.5 Å, which is the same distance we calculated in the C_{28} crystal at 2 K.

Thermal motion in these systems induces rotational mobility, which, in turn, gives wider bands in both angle distributions and density profiles and a greater distance between layers than is found at 2 K. At 300 K the interlayer distance increases to 4.0 Å. Visual inspection of the configurations

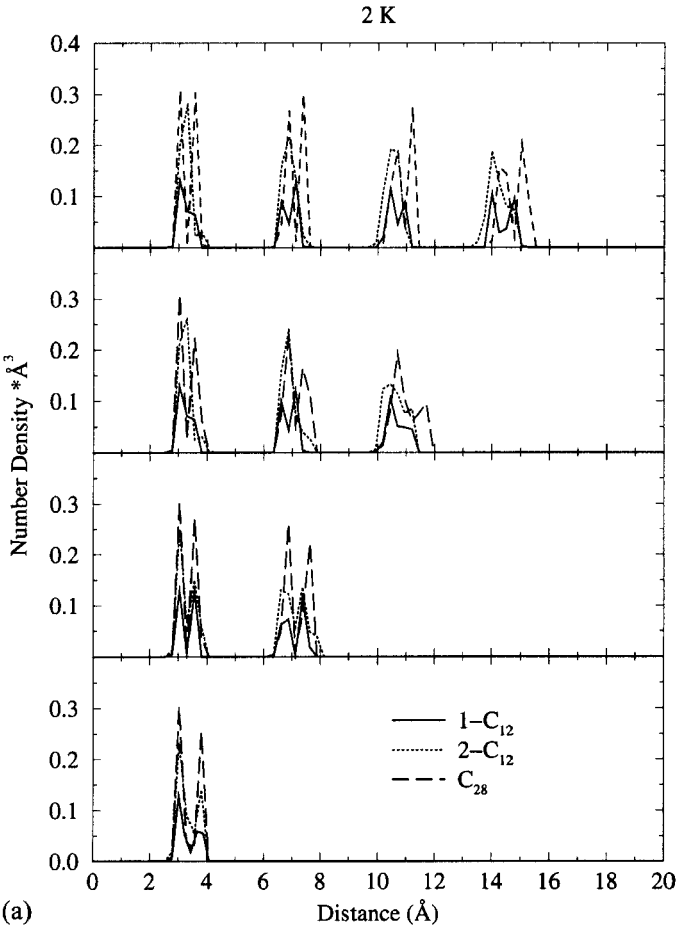

FIGURE 5 Normal density profiles of a single block (1-C_{12}) and two blocks (2-C_{12}) of thirty two C_{12} molecules and a single block of thirty two C_{28} molecules after relaxation at (a) 2 and (b) 300 K.

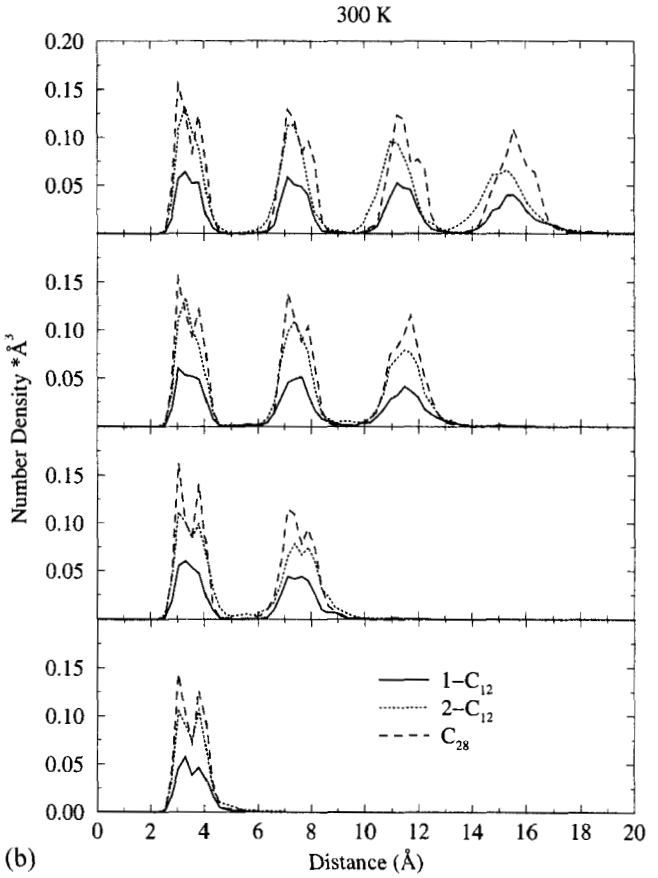

FIGURE 5 (Continued).

indicates that the ordering is conserved at this temperature, although some gauche defects do appear in the alkane chains. Table IV reports the percentage of gauche defects for every system. It is worth noting that C_{28} molecules retain a trans conformation better on increasing temperature than do the C_{12} molecules. In other respects the C_{28} and C_{12} systems with complete coverage are similar, with the layers occurring at much the same height above the surface, and with similar doublet resolutions. The C_{28} system does give a slightly larger interlayer separation for third and fourth layer, although this difference is less apparent at 300 K.

The double peaks in Figure 5 arise because the alkanes tilt relative to the surface. This can be seen clearly in Figure 4, and is seen to be more defined for 1-C_{12} and C_{28} than for 2-C_{12}. A similar tilt is also found in the

TABLE IV Percentage of gauche defects at 300 K

	Layer number	300 *K*
C_{28}-defect	1	3.0
	2	1.0
	3	1.8
	4	1.0
1-C_{12}	1	4.2
	2	4.9
	3	6.5
	4	4.9
2-C_{12}	1	4.2
	2	6.6
	3	5.3
	4	5.7

wax crystal (Fig. 2, (001) surface) but in the wax it alternates from layer to layer. The adsorbed layers also match the crystal in that each layer is offset from the layer beneath it. This layer structure corresponds to a growth along (010) direction.

The rotation about the alkane long axis has been analysed in more detail using the principal axes of each molecule. The moment of inertia matrix for each alkane was diagonalized and the eigenvector corresponding to the second largest eigenvalue, $\boldsymbol{e_2}$, used to define this tilt angle. Note that the eigenvector corresponding to the smallest eigenvalue, $\boldsymbol{e_3}$, defines the long axis of the molecule, while $\boldsymbol{e_2}$ is orthogonal to $\boldsymbol{e_3}$ and both eigenvectors lie within the alkane zig-zag plane for an all trans alkane conformation. The angle between $\boldsymbol{e_2}$ and the surface normal was then calculated for each molecule and used to construct angular frequency distributions. These are presented in the Figure 6. The angle has been averaged for all the molecules in each layer and at regular intervals (every 0.01 ps) during the last 10 ps of each simulation.

For dodecane it can be seen that the first layer adsorbed to the surface presents a wide distribution of angles. This will be discussed in more detail below. For subsequent layers the angle is well defined around 70° for the system with only one block of alkanes. The system with two blocks gives a more complex distribution of angles. The interaction between the two blocks induces reorientation of the angles. In particular the profile arising is different for every layer, although all the peaks appear in the range of 60–90°. With C_{28} one can observe a narrow angle distribution well defined between 50 and 70°, peaked at 60 and 65°.

We have analysed the C_{28} monolayer formation more closely, by considering different starting configurations. The molecules were placed as described above but modifying the angle between $\boldsymbol{e_2}$ and the normal surface.

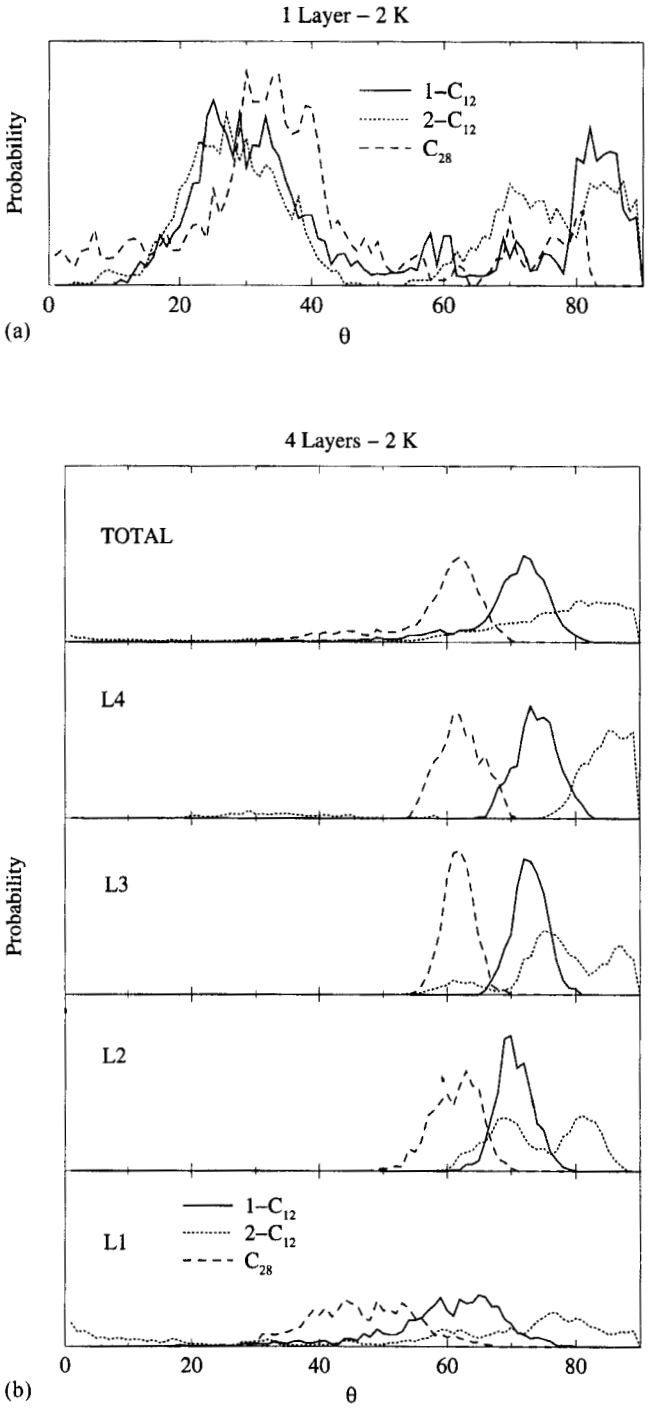

FIGURE 6 Distribution of alkane tilt angles for (a) one and (b) four layers of molecules in 1-C_{12}, 2-C_{12} and C_{28} systems at 2 K. See text for definition of θ.

It was found that after relaxation, the molecules rotated about their long axis leading to configurations with an angle distribution similar to that shown in the Figure 7, and with total energies that are comparable (*i.e.*, the maximal energy difference between two such these configurations was $5\,kJ\,mol^{-1}$ of C_{28}, or $0.2\,kJ\,mol^{-1}$ per carbon site). The reason why a unique angle is not found is because of the surface and the C_{28} crystal structure are incommensurate: the Fe_2O_3 surface provides slightly too much width in the *b* direction and so the driving force for efficient packing is smaller than would be the case in the alkane crystal. This interpretation will be justified in the next section.

3.2.2. Crystal-surface Interface

For comparison we have also modelled the ideal interface between the (010) surface of a C_{28} crystal and the (0001)-hematite surface. In order to get comparable results with those obtained from the 'ideal deposition', simulations were performed in NVT ensemble and the metal oxide surface atoms were fixed to the relaxed structure as described above. These alkane and hematite surfaces are incommensurate, although this mismatch is not large. We have therefore chosen to use a $7 \times 2 \times 1$ array of alkane unit cells which slightly undercovers the oxide surface: the 7×1 array for the (010) surface gives 39.0×38.2 Å compared with 40.3×40.3 Å for the oxide. Periodic boundaries for the calculation were defined by the oxide surface. The oxide and alkane slabs were initially separated by a vacuum gap of 7 Å, and allowed to relax at 2 K for 20 ps; this was sufficient time for the two surfaces to coalesce and then relax. After this time, two

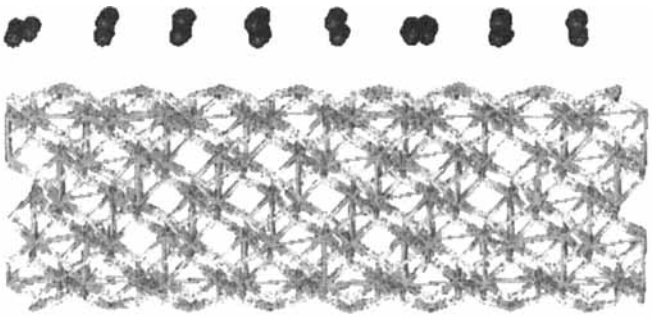

FIGURE 7 Side view of eight C_{28} molecules deposited on (0001)-Fe_2O_3 surface after relaxation at 2 K. Carbon atoms are in black, iron atoms in orange and oxygen atoms in grey. (See Color Plate III).

simulations were performed. The first one for 20 ps to analyse the properties at 2 K, and the second one for 20 ps at 300 K to examine the stability of the system at room temperature.

Figure 8 shows side and top views of the adsorbed alkane layer. The picture reveals that the molecules tend to lie between two iron rows. However, that disposition is only obtained for three molecules while the other four cross over an iron row; this happens because, after relaxation, the intralayer distance becomes bigger than the distance between iron rows, and so there is a mismatch between the alkane and iron row separations.

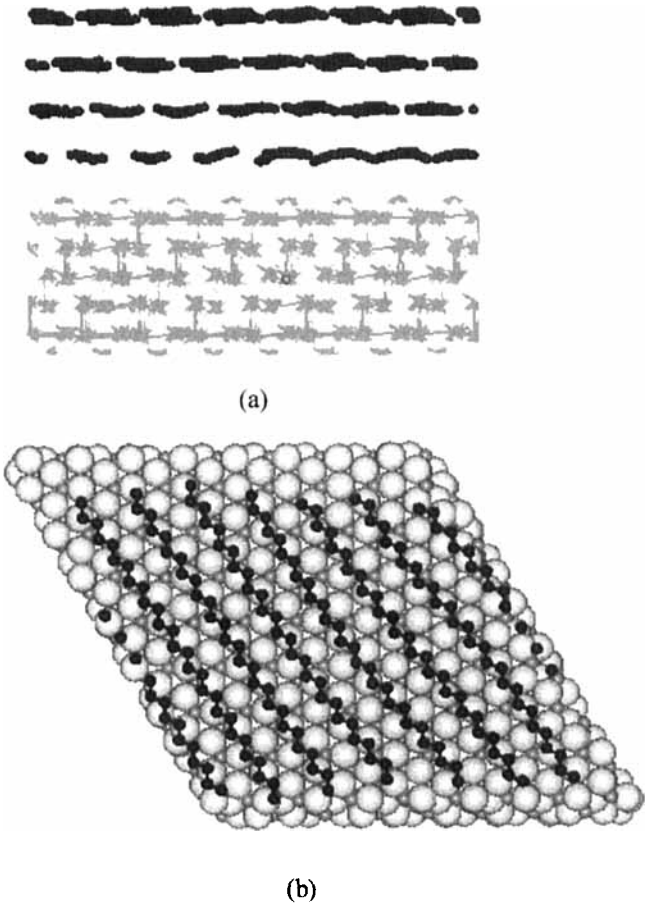

FIGURE 8 (a) Side view of C_{28}-crystal/hematite interface at 2 K. (b) Top view of the first layer adsorbed to the surface. Carbon atoms are in black and surface in orange (Fe) and grey (O). (See Color Plate IV).

The distributions of alkane tilt angles ($\cos\theta = \boldsymbol{e_2}\cdot\mathbf{n}$, where $\mathbf{n}$ is the surface normal) in Figure 9 shows a range of angles between 70 and 90° for every layer. This means the molecules rotate about their long axis, leading to an orientation that is almost parallel to the oxide surface. The effect occurs because the system dilates to occupy all the volume of the computational box, reducing the alkane density and allowing the rotation to a planar configuration at which the repulsive overlap interactions are minimised.

Radial distribution functions for the carbon–carbon distances in both systems are plotted in Figure 10. Most of the peaks in the curves correspond very closely, which indicates that the crystalline structures

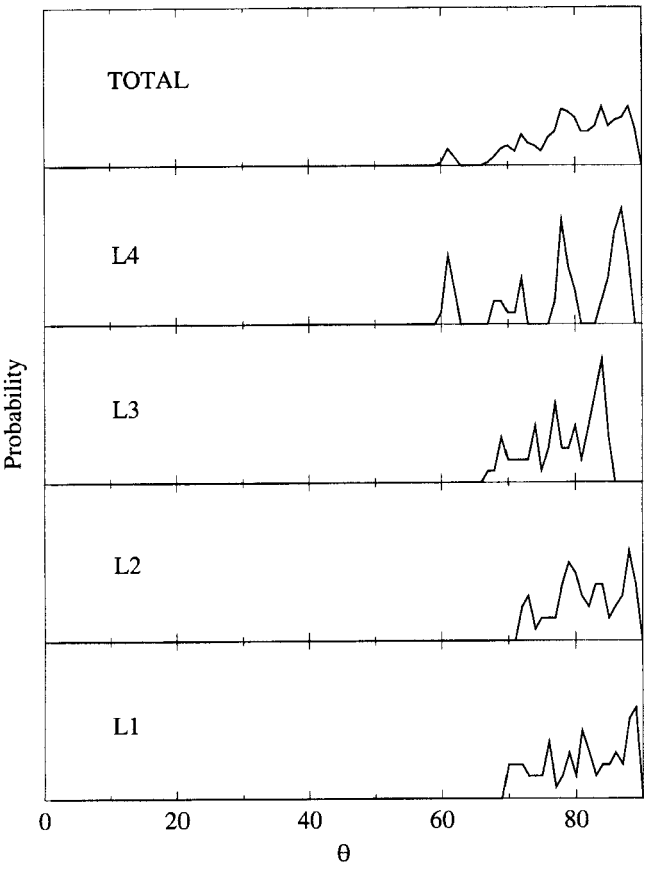

FIGURE 9 Distribution of alkane tilt angles for the separate four layers and the total distribution of a C_{28}-crystal on (0001)-hematite surface at 2 K.

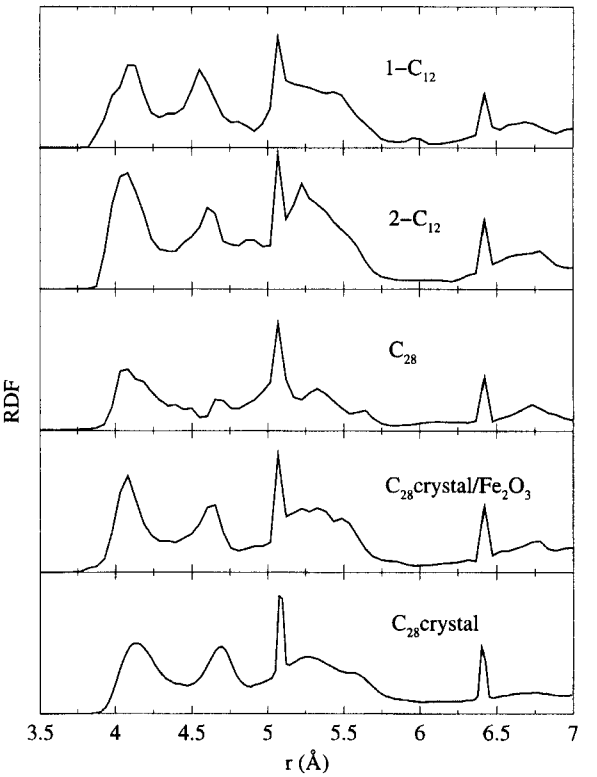

FIGURE 10 Radial distribution functions for 1-C_{12}, 2-C_{12}, C_{28} systems, C_{28} crystal and C_{28}-crystal/hematite interface relaxed at 2 K.

formed from the deposition are similar to the bulk C_{28} crystal. In particular, the C_{28} crystal and C_{28} crystal/Fe_2O_3 show no significant difference, indicating that the distortions induced by the oxide as described above have only a minor influence on the local structure in the alkane layer.

3.2.3. Random Deposition

In this part of the work we have considered the deposition of different numbers of C_{12} and C_{28} molecules on the (0001)-hematite surface. In order to obtain a random deposition process we have used the following protocol. A fixed number of molecules, n, was introduced into a simulation box, located 7 Å above the highest carbon atom (or the surface iron for the first addition) at different positions and random orientations. This system was

heated to 1000 K for 20 ps, rescaling velocities every 3 steps. A further 20 ps were then simulated at 300 K, again rescaling velocities every step. Finally a 100 ps simulation was performed to determine equilibrium properties. This procedure was iterated so that a further n alkanes were introduced into the final configuration from the last 100 ps run and the procedure

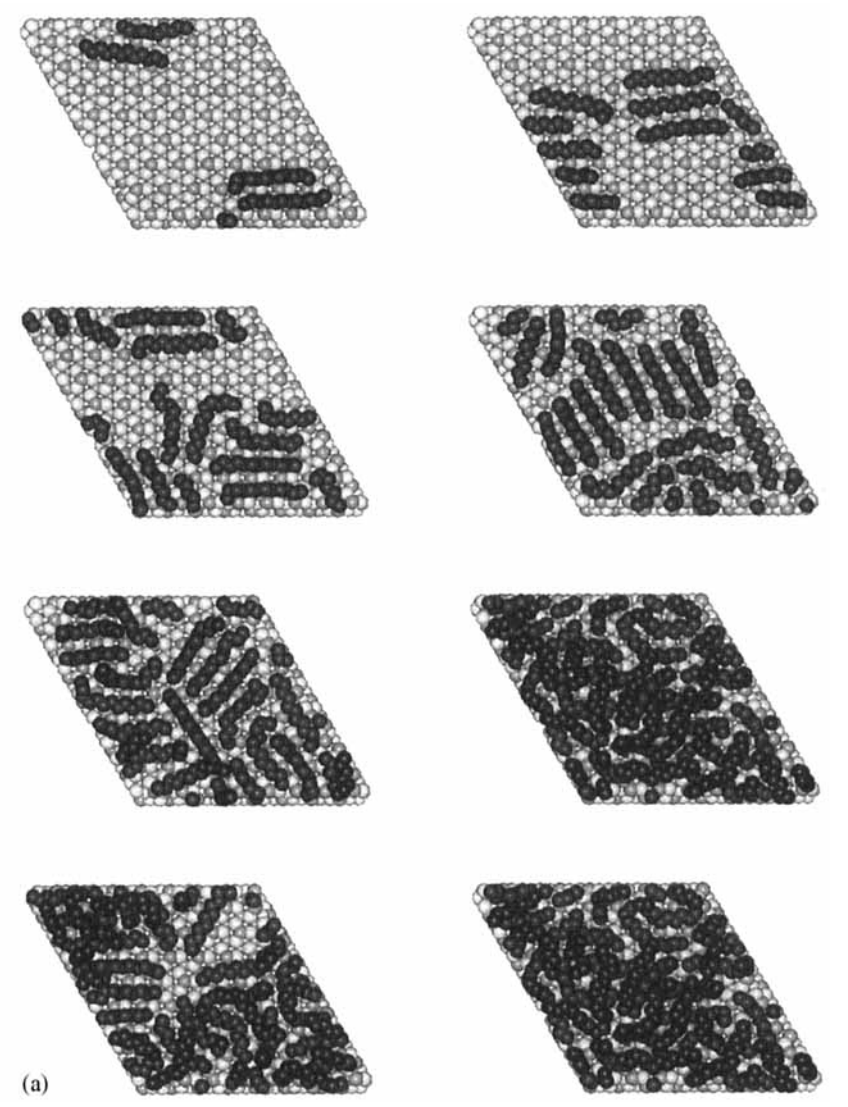

FIGURE 11 Snapshots of final configuration at 300 K for different numbers of C_{12} and C_{28} molecules on the (0001)-Fe_2O_3 surface, obtained using random deposition method. (See Color Plate V).

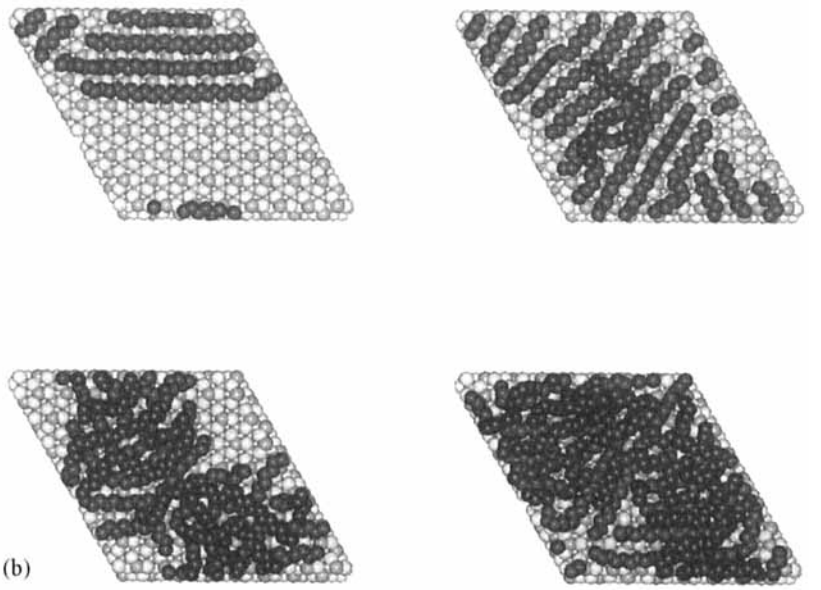

FIGURE 11 (Continued). (See Color Plate V).

repeated. For C_{12}, four molecules were added at each stage up to 32, while for C_{28}, four molecules were deposited each time up to a total of 16. These would correspond to two add-layers in an ideal system. The systems will be labelled as D*i* for dodecane and O*i* for octocosane, where *i* is total number of molecules added on to the oxide surface.

It should be noted that this protocol will introduce a number of gauche defects that would not be present in a better annealed system. The simulation at 1000 K is needed to allow an adequate exploration of the surface within a reasonable computer time, but does introduce gauche defects in a manner that is irreversible on the simulation time scale. In general the method was found to increase the number of defects by one order of magnitude over ideal deposition.

Figure 11 shows a snapshot of the final configuration for every system. It can be seen that the molecules tend to cluster by rotating about their long axis in a similar way to that found in the 'ideal deposition'. For C_{12}, all the molecules belong to the first layer up to coverage of D20. This gives a substantially higher packing density than was considered in the 'ideal adsorption' method. For C_{28} the allocation of the molecules is more difficult due to the longer chain, however in O8 the molecules are well ordered and orient parallel to each other.

From the density profiles in Figure 12 it is possible to see the formation of different layers on increasing the number of molecules deposited on the surface. The intralayer distance is 4 Å, as found in ideal deposition at 300 K. There is also some evidence of a doublet peak for the first layer, indicating a tilt of the zig-zag plane, again as found for ideal deposition.

Figure 13 shows the percentage of gauche defects for every system at 300 K as a function of the number of carbon atoms. The behaviour of the both systems is similar. The number of defects is quite reduced up to D12

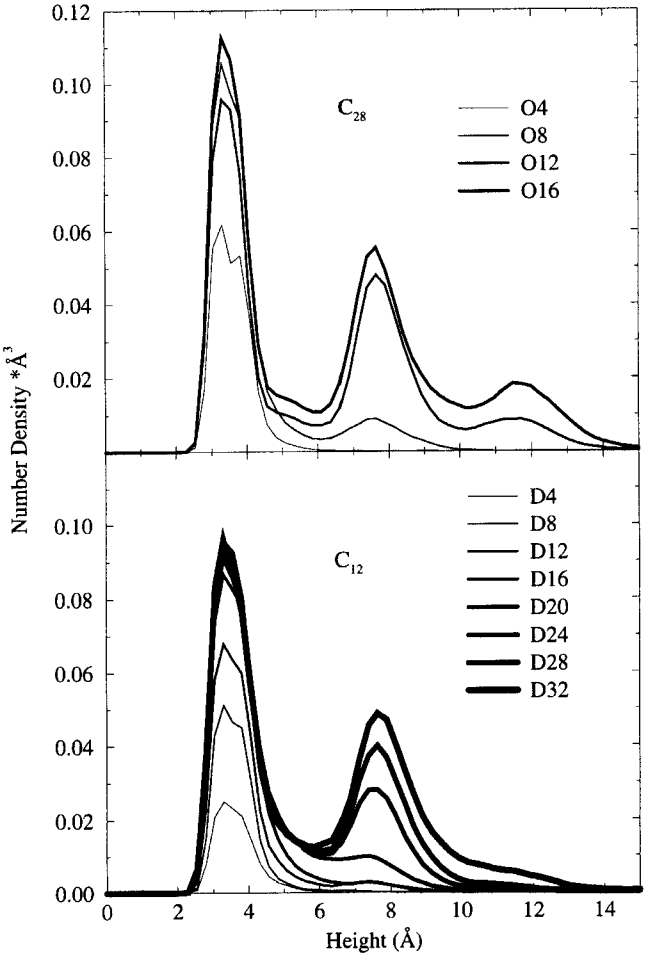

FIGURE 12 Normal density profiles of different numbers of C_{12} and C_{28} molecules on the (0001)-Fe_2O_3 surface at 300 K, obtained using random deposition method.

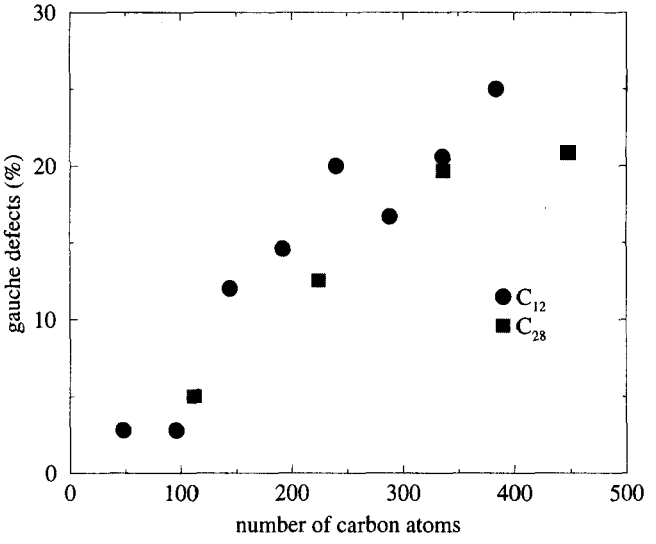

FIGURE 13 Percentage of gauche defects of C_{12} and C_{28} molecules on (0001)-Fe_2O_3 surface at 300 K.

or O4 because the molecules are adsorbed to the surface adequately as was described earlier. On increasing the number of carbon atoms, the allocation is more difficult and some particles jump to the second layer to reduce the interactions with the neighbouring atoms and consequently inducing gauche defects.

4. CONCLUSIONS

MD simulations have been performed to obtain a model of the relaxed (0001)-hematite surface, which is expected to be the most common exposed surface on pipeline walls. We have studied the adsorption of C_{28} and C_{12} alkanes on this surface. For adsorption of a single molecule, the molecule lies parallel to the surface and zig-zags between the protruding iron atoms.

We have simulated crystal growth by considering two different methods. The first consisted of the deposition of molecules onto the adsorption sites a layer at a time, giving up to four layers. This yielded a structure comparable with the C_{28} crystal, with the same interlayer distance and a characteristic crystalline tilt angle around the long axis. The second procedure involved siting the molecules randomly and allowing the system to relax at 300 K. Up to monolayer coverage it was observed that the add-molecules

tended to cluster, forming a monolayer of parallel alkanes and utilising the adsorption sites found with the single molecule. The subsequent deposition of additional molecules generates a second layer with a layer separation of 4 Å, as was found at this temperature with the first procedure. The system produced with the second procedure shows a distinct tendency to form a crystalline structure although a perfect crystal is not formed due to limitations such as the exhaustive simulation time that would be required for complete annealing.

We have also examined the match between a C_{28} crystal and the (0001)-hematite surface. We have found that, despite the two surfaces being not quite commensurate, the structure of the interface is comparable to that found in the simulated deposition processes, and the alkane side of the interface does adopt a structure that corresponds closely with that of bulk alkane crystals.

From these results we can conclude that the (0001)-hematite surface presents a suitable structure that allows the crystal growth of waxes along one of the most favourable directions.

Acknowledgements

This work was supported through EPSRC grant GR/L73739.

References

[1] Harrob, D., BP Exploration, private communications.
[2] de Sainte Claire, P., Hass, K. C., Schneider, W. F. and Hase, W. L. (1997). "Simulations of hydrocarbon adsorption and subsequent water penetration on an aluminium oxide surface", *J. Chem. Phys.*, **106**, 7331.
[3] Bolton, K., Bosio, S. B. M., Hase, W. L., Schneider, W. F. and Hass, K. C. (1999). "Comparison of explicit and united atom models for alkane chains physisorbed on α-Al_2O_3 (0001)", *J. Phys. Chem. B*, **103**, 3885.
[4] Huang, D., Chen, Y. and Fichthorn, K. A. (1994). "A molecular-dynamics simulation study of the adsorption and diffusion dynamics of short *n*-alkanes on Pt(111)", *J. Chem. Phys.*, **101**, 11021.
[5] Huang, D., Balan, P. G., Chen, Y. and Fichthorn, K. A. (1994). "Molecular-dynamics simulation of the surface-diffusion of *n*-alkanes on Pt(111)", *Mol. Simul.*, **13**, 285.
[6] Fichthorn, K. A., Balan, P. G. and Chen, Y. (1994). "Simulation and analysis of the motion of *n*-butane on Pt(111)", *Surf. Sci.*, **317**, 37.
[7] Balasubramanian, S., Klein, M. L. and Siepmann, J. I. (1996). "*Simulation studies of ultrathin films of linear and branched alkanes on a metal substrate*", **100**, 11960.
[8] Balasubramanian, S., Klein, M. L. and Siepmann, J. I. (1995). "Monte-Carlo investigations of hexadecane films on a metal-substrate", *J. Chem. Phys.*, **103**, 3184.
[9] Xia, T. K. and Landman, U. (1993). "Molecular-Dynamics of adsorption and segregation from an alkane mixture", *Science*, **261**, 1310.
[10] Cohen, D. and Zeiri, Y. (1992). "A theoretical-study of the surface-diffusion of large molecules. 1. Normal-alkane-type chains on W(100)", *J. Chem. Phys.*, **97**, 1531.

[11] Mundy, C. J., Balasubramanian, S., Bagchi, K., Siepmann, J. I. and Klein, M. L. (1996). "Equilibrium and non-equilibrium simulation studies of fluid alkanes in bulk and at interfaces", *Faraday Discussions*, **104**, 17.
[12] Hentschke, R., Schurmann, B. L. and Rabe, J. P. (1992). "Molecular-dynamics simulations of ordered alkane chains physisorbed on graphite", *J. Chem. Phys.*, **96**, 6213.
[13] Hansen, F. Y. and Taub, H. (1999). "The mechanism of melting in monolayer films of short and intermediate-length *n*-alkanes adsorbed on graphite", *Inorganic Materials*, **35**, 586.
[14] Peters, G. H. and Tildesley, D. J. (1996). "Molecular Dynamics simulations of the melting of a hexane monolayer: isotropic *versus* anisotropic force fields", *Langmuir*, **12**, 1557.
[15] Uhlig, H. H. and Revie, R. W., *Corrosion and Corrosion Control*, 3rd, edn.; John Wiley and Sons: New York, 1985.
[16] Finger, L. W. and Hazen, R. M. (1980). "Crystal structure and isothermal compression of Fe_2O_3, Cr_2O_3, and V_2O_3 to 50 kbars", *J. Appl. Phys.*, **51**, 5362.
[17] Fujimori, A., Saeki, M., Kimizuka, N., Taniguchi, M. and Suga, S. (1986). "Photoemission satellites and electronic-structure of Fe_2O_3", *Phys. Rev. B*, **34**, 7318.
[18] Nagel, S., "Cluster calculation of electronic-structure and hyperfine interactions for α-Fe_2O_3", *J. Phys. Chem. Solids*, **46**, 905.
[19] Sherman, D. M. (1985). "The electronic structures of Fe^{3+} coordination sites in iron oxides; applications to spectra, bonding, and magnetism", *Phys. Chem. Miner.*, **12**, 161.
[20] Catti, M., Valerio, G. and Dovesi, R. (1995). "Theoretical study of electronic, magnetic, and structural properties of α-Fe_2O_3 (hematite)", *Phys. Rev. B*, **51**, 7441.
[21] Lad, R. J. and Henrich, E. (1988). "Structure of α-Fe_2O_3 single crystal surfaces following Ar^+ ion bombardment and annealing in O_2", *Surf. Sci.*, **193**, 81.
[22] Eggleston, C. M. and Hochella, M. F. (1992). "The structure of hematite {001} surfaces by scanning tunneling microscopy: image interpretation, surface relaxation, and step structure", *American Mineralogist*, **77**, 911.
[23] Guo, Q. and Moller, P. J. (1995). "HREELS and LEED studies on Cu deposited on 1×1 reconstructed α-Fe_2O_3 (0001) surfaces", *Surf. Sci.*, **340**, L999.
[24] Condon, N. G., Leibsle, F. M., Lennie, A. R., Murray, P. W., Parker, T. M., Vaughan, D. J. and Thornton, G., "Scanning tunnelling microscopy studies of α-Fe_2O_3 (0001)", *Surf. Sci.*, **397**, 278.
[25] Mackrodt, W. C., Davey, R. J., Black, S. N. and Docherty, R. (1987). "The morphology of α-Al_2O_3 and α-Fe_2O_3: the importance of surface relaxation", *J. Crystal Growth*, **80**, 441.
[26] Hartman, P. (1989). "The effect of surface relaxation on crystal habit: cases of corundum (α-Al_2O_3) and hematite (α-Fe_2O_3)", *J. Crystal Growth*, **96**, 667.
[27] Mackrodt, W. C. (1989). "Atomistic simulation of the surfaces of oxides", *J. Chem. Soc., Faraday Trans. 2*, **85**, 541.
[28] Wasserman, E., Rustad, J. R., Felmy, A. R., Hay, B. P. and Halley, J. W. (1997). "Ewald methods for polarizable surfaces with application to hydroxylation and hydrogen bonding on the (012) and (001) surfaces of α-Fe_2O_3", *Surf. Sci.*, **385**, 217.
[29] Smith, W. and Forester, T. R. (1996). *J. Mol. Graphics*, **14**, 136.
[30] Shannon, R. D. and Prewitt, C. T. (1969). *Acta Crystallogr., Sect. B: Struct. Crystallogr. Cryst. Chem. B*, **25**, 925.
[31] Kurtz, R. L. and Henrich, V. E. (1987). "Surface electronic structure and chemisorption on corundum transition-metal oxides: α-Fe_2O_3", *Phys. Rev. B*, **36**, 3413.
[32] Godwin, P. D. and Rodger, P. M., private communication.
[33] Duffy, D. M. and Rodger, P. M., submitted to *Phys. Chem. Chem. Phys.*
[34] McGann, M. R. and Lacks, D. J. (1999). "Chain length effects on the thermodynamic properties of *n*-alkane crystals", *J. Phys. Chem. B*, **103**, 2796.
[35] Moller, M. A., Tildesley, D. J., Kim, K. S. and Quirke, N. (1991). "Molecular dynamics simulation of a Langmuir-Blodgett film", *J. Chem. Phys.*, **94**, 8390.